Molecular Systems Biology (2006) doi:10.1038/msb4100068

www.molecularsystemsbiology.com
2006.0033

molecular systems biology

Oscillations and variability in the p53 system

Naama Geva-Zatorsky[1,3], Nitzan Rosenfeld[1,3], Shalev Itzkovitz[1], Ron Milo[1], Alex Sigal[1], Erez Dekel[1], Talia Yarnitzky[1], Yuvalal Liron[1], Paz Polak[1], Galit Lahav[2] and Uri Alon[1,*]

[1] Department of Molecular Cell Biology, Weizmann Institute of Science, Rehovot, Israel and [2] Department of Systems Biology, Harvard Medical School, Boston, MA, USA
* Corresponding author. Molecular Cell Biology and Physics of Complex Systems, Weizmann Institute of Science, Rehovot 76100, Israel.
Tel.: +972 8 9344448; Fax: +972 8 9344125; E-mail: urialon@weizmann.ac.il
[3] These authors contributed equally to this work

Received 5.8.05; accepted 28.3.06

Understanding the dynamics and variability of protein circuitry requires accurate measurements in living cells as well as theoretical models. To address this, we employed one of the best-studied protein circuits in human cells, the negative feedback loop between the tumor suppressor p53 and the oncogene Mdm2. We measured the dynamics of fluorescently tagged p53 and Mdm2 over several days in individual living cells. We found that isogenic cells in the same environment behaved in highly variable ways following DNA-damaging gamma irradiation: some cells showed undamped oscillations for at least 3 days (more than 10 peaks). The amplitude of the oscillations was much more variable than the period. Sister cells continued to oscillate in a correlated way after cell division, but lost correlation after about 11 h on average. Other cells showed low-frequency fluctuations that did not resemble oscillations. We also analyzed different families of mathematical models of the system, including a novel checkpoint mechanism. The models point to the possible source of the variability in the oscillations: low-frequency noise in protein production rates, rather than noise in other parameters such as degradation rates. This study provides a view of the extensive variability of the behavior of a protein circuit in living human cells, both from cell to cell and in the same cell over time.
Molecular Systems Biology 13 June 2006; doi:10.1038/msb4100068
Subject Categories: metabolic & regulatory networks
Keywords: cancer genetics; fluorescence microscopy; quantitative biology; systems biology

Introduction

A goal of systems biology is to understand the design principles that govern dynamics of protein regulatory circuits (Hartwell *et al*, 1999). It is especially important to investigate network motifs, regulatory patterns that recur in various biological networks (Milo *et al*, 2002; Alon, 2003, 2006). Understanding the dynamical features of a specific network motif may help us to understand diverse biological systems in which this motif appears (Lee *et al*, 2002; Shen-Orr *et al*, 2002; Mangan and Alon, 2003; Kalir and Alon, 2004; Odom *et al*, 2004; Boyer *et al*, 2005; Ma'ayan *et al*, 2005; Mangan *et al*, 2006). For this purpose, it is important to study the best-characterized systems using dynamic measurements in living cells.

To understand protein circuits, it is important to study the impact of the stochastic nature of biological reactions on the behavior of the circuit (Novick and Weiner, 1957; Spudich and Koshland, 1976; McAdams and Arkin, 1997, 1999; Becskei and Serrano, 2000; Thattai and van Oudenaarden, 2001; Elowitz *et al*, 2002; Hasty *et al*, 2002; Ozbudak *et al*, 2002; Blake *et al*, 2003; Isaacs *et al*, 2003; Paulsson, 2004; Raser and O'Shea, 2004, 2005; Becskei *et al*, 2005; Blake and Collins, 2005; Colman-Lerner *et al*, 2005; Golding *et al*, 2005; Kaern *et al*, 2005; Sachs *et al*, 2005; Weinberger *et al*, 2005; Volfson *et al*, 2006). For this purpose, it is essential to study individual cells and to measure the cell–cell variations in the biological response, rather than averaging over cell populations. Most studies of stochastic behavior to date have been in micro-organisms. It would therefore be of interest to measure the behavior and variability of a protein circuit over long times in individual human cells.

Here, we study the dynamics and variability of one of the network motifs that recurs across organisms: a negative feedback loop, which is composed of interactions on two different timescales—a slow positive transcriptional arm and a fast negative protein–protein interaction arm (Lahav *et al*, 2004; Yeger-Lotem *et al*, 2004; Ma'ayan *et al*, 2005). We study this network motif within one of the best-characterized systems in human cells, the negative feedback loop between p53 and Mdm2 (Kubbutat and Vousden, 1998; Prives, 1998; Larkin and Jackson, 1999; Prives and Hall, 1999; Vogelstein *et al*, 2000; Ryan *et al*, 2001; Vousden and Lu, 2002; Oren, 2003; Meek, 2004; Bond *et al*, 2005; Harris and Levine, 2005).

In the p53 system, p53 transcriptionally activates *mdm2*. Mdm2, in turn, negatively regulates p53 by both inhibiting its activity as a transcription factor and by enhancing its degradation rate (Barak *et al*, 1993; Wu *et al*, 1993; Haupt *et al*,

1997; Kubbutat *et al*, 1997; Piette *et al*, 1997; Momand *et al*, 2000). The concentration of p53 increases in response to stress signals, such as DNA damage. The main mechanism for this increase is stabilization of p53 due to reduced interaction with Mdm2. Following stress signals, p53 activates transcription of several hundred genes that are involved in growth arrest, apoptosis, senescence, and DNA repair. It is important to note that many additional proteins interact with p53 and Mdm2, so that the negative feedback loop motif is embedded inside a network of additional interactions, many of which are not fully characterized (Harris and Levine, 2005).

Models of negative feedback loops, such as between p53 and Mdm2, suggest that they can generate an oscillatory behavior with a time delay between the two proteins (Lev Bar-Or *et al*, 2000; Mihalas *et al*, 2000; Hoffmann *et al*, 2002; Tiana *et al*, 2002; Michael and Oren, 2003; Monk, 2003; Tyson *et al*, 2003; Nelson *et al*, 2004; Tyson, 2004; Ciliberto *et al*, 2005; Ma *et al*, 2005). For different parameters of the feedback loop, the dynamics can show either a monotonic response, damped oscillations, or undamped (sustained) oscillations in which each peak has the same amplitude as the previous peak (Lahav, 2004). The stronger the interactions between the proteins, the more oscillatory the dynamics. Other parameters, such as high basal degradation rates of the proteins, tend to damp out the oscillations. Most models of the p53 network used deterministic equations, and thus did not consider the cell–cell variability in the dynamics.

Experimental studies have shown that p53 and Mdm2 undergo oscillatory behavior following DNA damage caused by gamma irradiation. These oscillations appeared to be damped in assays that measure averages over population of cells (Lev Bar-Or *et al*, 2000). In a previous study, we developed a system for following p53 and Mdm2 dynamics in individual living cells. This system used an MCF7 breast cancer cell line stably transfected with p53 fused to cyan fluorescent protein (CFP), and Mdm2 fused to yellow fluorescent protein (YFP). The p53-CFP fusion protein was active in causing apoptosis and transactivating downstream targets. The concentrations and dynamics of both fluorescently tagged proteins were found in Western blots to reliably reproduce the concentration and dynamics of the endogenous p53 and Mdm2 expressed by these cells (Lahav *et al*, 2004). In our previous study, individual cell measurements using fluorescent microscopy were limited to 16 h following gamma irradiation. During this 16 h period, we observed up to two undamped peaks of p53-CFP concentration following gamma irradiation (Lahav *et al*, 2004). The peak amplitude and timing did not depend on the dose of irradiation. The mean number of peaks appeared to increase with irradiation dose, in the sense that the probability for two peaks in the 16 h experiment increased with dose, whereas the probability for no oscillation peaks decreased with dose.

Here, we experimentally investigate p53 and Mdm2 dynamics in individual living breast cancer (MCF7) cells for much longer times than in our previous study. In a large fraction of cells, we find sustained undamped oscillations of p53-CFP and Mdm2-YFP, which lasted for at least $\sim$3 days following gamma irradiation. We also extend our previous study by examining the noise in the response. We find that the oscillation pattern was highly variable between isogenic cells, but this variation had distinct properties: the oscillation amplitudes fluctuated widely, yet the oscillation frequency was much less variable. In addition to cells that oscillated, other cells showed a dynamic fluctuation of protein levels that did not resemble sustained oscillations. The prolonged experiments indicate that the fraction of oscillating cells increases with irradiation dose.

We also present a theoretical analysis of the negative feedback loop in the p53 system. We extend previous theoretical studies by investigating several families of models, and by studying the effect of stochasticity in the model reactions. We find that several distinct model families can capture the experimentally observed oscillations, and suggest 'consensus parameters' for *in vivo* degradation and production rates in this system. To capture the variability in the dynamics, we find that one must explicitly add long-wavelength noise to different model parameters. The analysis indicates that the observed characteristic variation in the oscillations stems from fluctuations in the protein production rates, rather than from fluctuations in other parameters. Essentially, the negative feedback loop amplifies slowly varying noise in the protein production rates at frequencies near the resonance frequency of the feedback loop.

Results

Prolonged time-lapse movies show undamped oscillations over days

We used an MCF7 cell line clone stably transfected with p53-CFP and Mdm2-YFP (Lahav *et al*, 2004). The results we describe were obtained from isogenic cells, grown from a single parental cell (Lahav *et al*, 2004). Western blots indicate that the concentration of exogenous p53-CFP and Mdm2-YFP protein in our cell line is comparable to the endogenous p53 and Mdm2 protein concentration (Lahav *et al*, 2004). Hence, these proteins are not strongly overexpressed in the present system.

We obtained time-lapse fluorescence microscopy movies of these cells for extended periods of time after exposure to gamma irradiation (Figure 1A and movie SM1 in Supplementary information). Overall, we collected time courses from over 1000 individual cells in different experiments with different doses of gamma irradiation. Most of the time-lapse movies were performed in an incubator environment with controlled humidity, temperature, and CO_2, providing conditions that allow growth over several days. Every 10–20 min, images of the cells in fluorescence and phase illumination were captured. Cells divided vigorously in the movies without gamma irradiation for at least 3 days. Gamma irradiation caused cells to enter growth arrest. We found that p53-CFP and Mdm2-YFP fluorescence was brightly visible when the proteins were in the cell nucleus (Figure 1A and Supplementary Figure S1). For each cell, we obtained a time-dependent signal equal to the mean fluorescence intensity of p53-CFP and Mdm2-YFP in the nucleus (Figures 1 and 2 and Supplementary Figure S2).

Nuclear levels of p53-CFP and Mdm2-YFP were found to oscillate continuously following gamma irradiation in a large

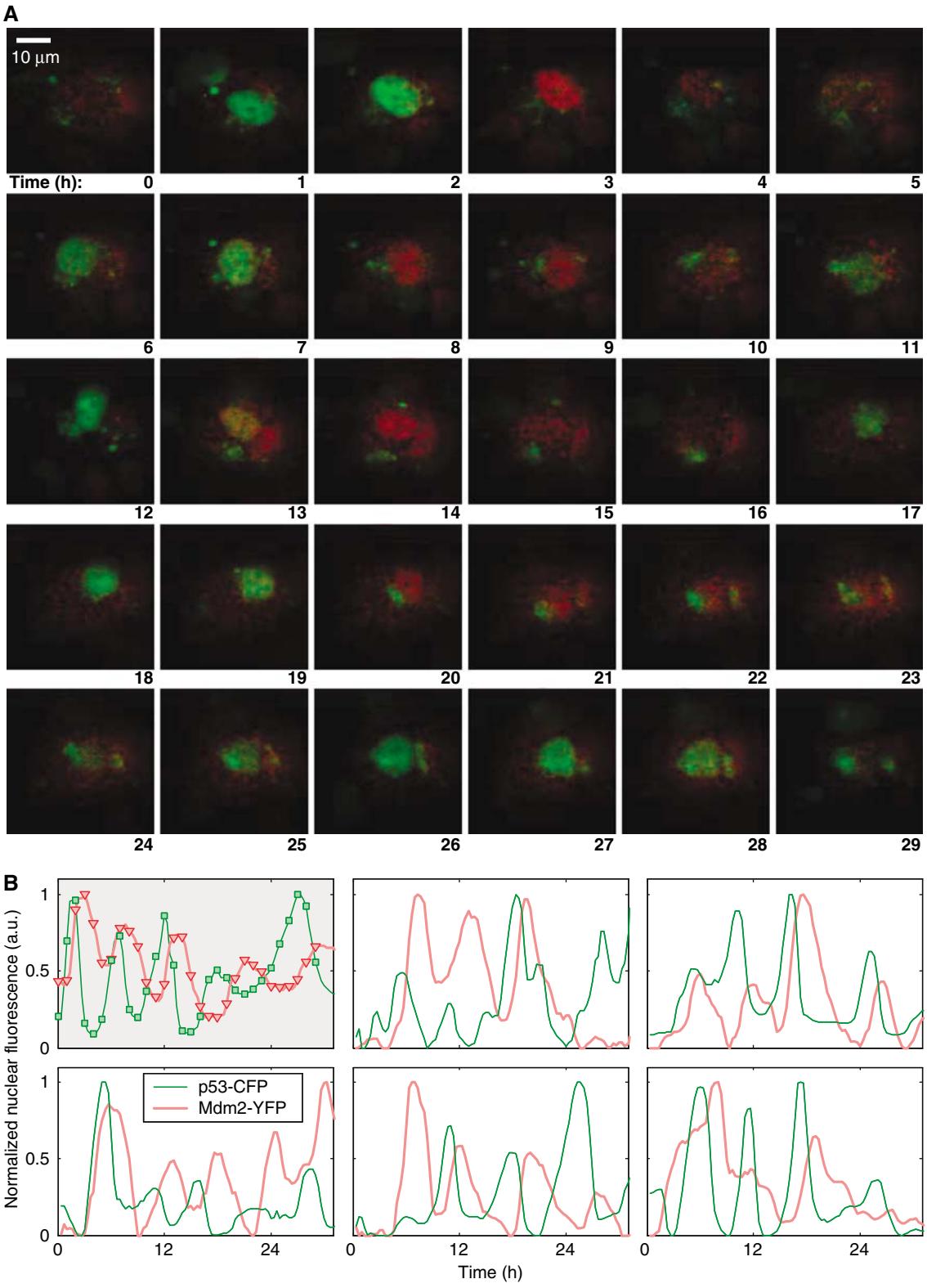

Figure 1 Prolonged oscillations in the nuclear levels of fluorescently tagged p53 and Mdm2 in individual MCF7, U280, cells following gamma irradiation. (**A**) Time-lapse fluorescence images of one cell over 29 h after 5 Gy of gamma irradiation. Nuclear p53-CFP and Mdm2-YFP are imaged in green and red, respectively. Time is indicated in hours. (**B**) Normalized nuclear fluorescence levels of p53-CFP (green) and Mdm2-YFP (red) following gamma irradiation. Top left: the cell shown in panel A. Other panels: five cells from one field of view, after exposure to 2.5 Gy gamma irradiation.

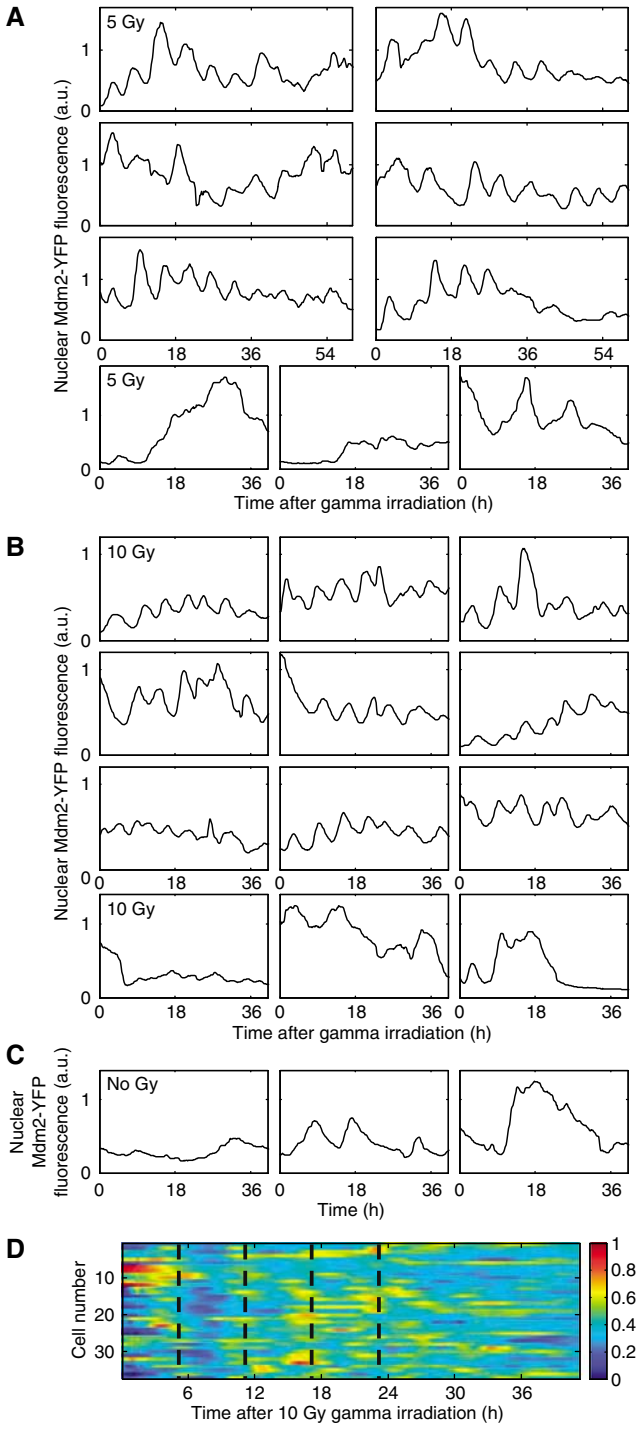

Figure 2 Nuclear Mdm2-YFP fluorescence in MCF7 cells, U280. (**A, B**) Oscillations in Mdm2-YFP levels after exposure to 5 Gy (A) and 10 Gy (B) of gamma irradiation. The bottom three panels in (A) and (B) are non-oscillatory cells. (**C**) Mdm2-YFP dynamics without gamma irradiation. (**D**) Timing of the nuclear Mdm2-YFP peaks: the horizontal lines show the normalized Mdm2-YFP dynamics over time for 37 cells with ~5.5-h oscillations. Blue hues indicate low fluorescence levels and yellow-reddish colors indicate high fluorescence levels. Dotted vertical lines are a guide to the eye, indicating 6-h intervals.

number of cells. In most of these cells, these oscillations lasted for the entire movie duration (Figures 1 and 2).

We analyzed the characteristic oscillation frequency in each cell using Fourier analysis (Supplementary Figure S3) and pitch detection, a method commonly used for determining principal frequencies in noisy non-stationary signals in the context of speech recognition (see Materials and methods). In long movies, we found that about 60% of the cells exposed to a pulse of 10 Gy gamma irradiation showed sustained Mdm2-YFP oscillations, with a period of 5.5 ± 1.5 h (Figure 3).

It is important to note that a significant fraction of the cells (about 40% in 10 Gy) showed Mdm2-YFP dynamics that did not resemble sustained oscillations (Figure 2 and Supplementary Figure S2). These cells showed either no response or slowly varying fluctuations (Figure 2A and B, bottom panels). In a few cells, the oscillations stopped or changed frequency after 1–2 days.

The onset of oscillations in different cells was synchronized to the DNA damage signal. Cells gradually lost synchrony with each other owing to the variations in oscillation frequencies (Figure 2D and Supplementary Figure S2E). In oscillating cells, Mdm2-YFP peaks followed p53-CFP peaks at a delay of 2 ± 0.5 h on average (Figures 1 and 4C).

We evaluated the amplitude and width of each peak in each oscillating cell, and calculated the average of these properties. The average amplitude of the oscillations did not appear to change significantly over time (Figure 4A). Similarly, the mean peak width did not change considerably throughout the movies (Figure 4B). In this sense, the oscillations can be described as undamped.

Peak amplitude is highly variable, whereas peak timing is more precise

The dynamics of cells from a clone in the same field of view showed significant cell–cell differences. These differences were seen between different cells, and also between different peaks in the same cell. We examined the variability between peaks in the oscillations (e.g. Figure 1B). We found that the amplitudes of the individual peaks varied with a coefficient of variance (standard deviation divided by mean) of about 70% (Figure 4D). The amplitudes of Mdm2-YFP peaks were not correlated to the amplitude of the preceding or the subsequent p53-CFP peaks (correlation coefficient of 0 ± 0.2). In some cases, Mdm2-YFP peaks occurred without a detectable preceding p53-CFP peak (Supplementary Figure S4).

In contrast to the large variability in amplitude, the peak width and p53–Mdm2 delay of individual peaks were more constant and varied by only about 30% (Figure 4E and F). The variation in the oscillation period for each cell (change of pitch value along the oscillation signal) was less than 20% in most oscillating cells.

Correlation between sister cells is lost within half a generation

To further study the variability in the dynamics of each cell, we examined cells that underwent cell division during the movie.

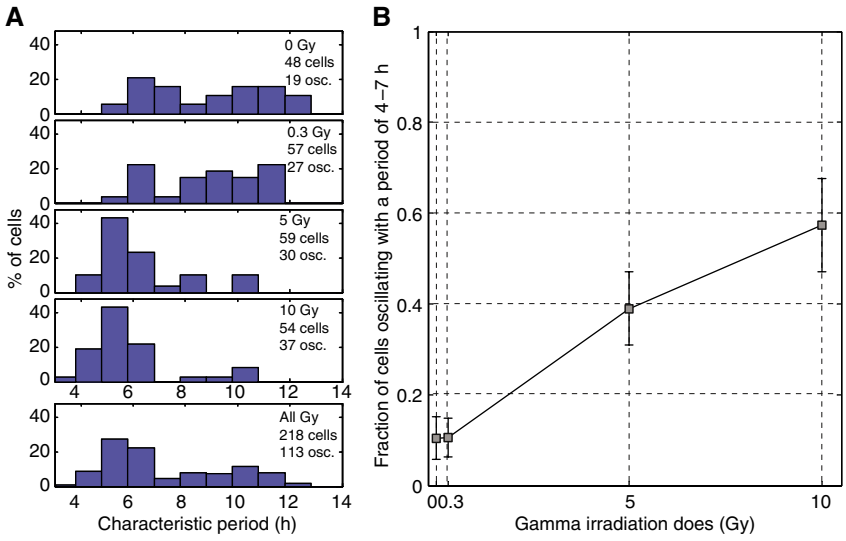

Figure 3 Pitch (characteristic period) of Mdm2-YFP signals of cells at various gamma irradiation doses. (**A**) Histogram of the pitch values from movies of cells exposed to 0, 0.3, 5, and 10 Gy, and from all the movies together. For each movie, the total number of cells is indicated, and the number of oscillating (osc.) cells that had a detectable pitch. (**B**) Fraction of cells (out of the total number of cells) with a pitch value of 4–7 h, for different gamma doses. Black line is a guide to the eye.

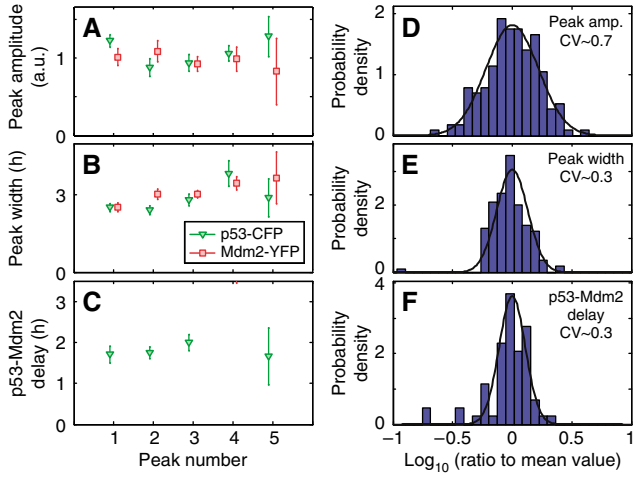

Figure 4 Average amplitude, width, and time delay of oscillation peaks and their variance. (**A–C**) Average values of the first five p53-CFP (green triangles) and Mdm2-YFP (red squares) oscillation peaks in 146 cells exposed to 5 Gy of gamma irradiation, shown with their standard errors. (A) Average oscillation amplitude of each of the first five peaks (peak to trough). (B) Average width (full-width half-maximum). (C) Average time delay between the p53 peaks and the consecutive Mdm2 peak. (**D–F**) The distribution of the individual peak amplitude, width, and delay divided by the mean value (note log scale). Black line: Log-normal probability distribution function, with mean=0 and standard deviation=0.22 (D), 0.13 (E), and 0.11 (F). The coefficient of variation (CV) of the original (not log) distribution is indicated.

In the first 40 h of the movies, these comprised ~75% of the non-irradiated cells, ~65% of the cells following 0.3 Gy, ~50% of the cells following 5 Gy, and ~10% of the cells following 10 Gy of gamma irradiation. Six typical examples are shown in Figure 5A.

We analyzed over 100 sister-cell pairs following cell division (see Materials and methods). We found that after division, the dynamics of Mdm2-YFP were correlated between sister cells for a few hours. This correlation was reduced by 50% within about 11 ± 5 h on average (Figure 5B). No significant correlation of the dynamics with the cell cycle was observed in these cells.

Some cells show non-oscillatory fluctuations

We found that a fraction of both irradiated cells and non-irradiated cells showed Mdm2-YFP signals that had slowly varying fluctuations that did not resemble oscillations (Figure 2 and Supplementary Figure S2). The fluctuations were rather slow, with a typical timescales of 8–12 h, as determined by Fourier analysis and pitch-detection methods (Figure 3). The fluctuations showed at most 2–3 such peaks rather than sustained oscillations (Figure 2A–C and Supplementary Figure S2). Similar fluctuations were also observed in p53-CFP (data not shown). Control cells expressing a YFP fusion protein (YFP fused to histone H2AZ), showed no such fluctuations (data not shown).

Fraction of cells with ~5.5-h oscillations increases with gamma dose

We also measured the dynamics under different doses of irradiation. When gamma irradiation was applied at 0.3 or 5 Gy, a fraction of the cells displayed oscillations with a period of about 5.5 h, similar to those in the 10 Gy experiment. We used pitch detection to estimate the fraction of cells whose characteristic period is 4–7 h. We found that the fraction of cells that perform Mdm2-YFP oscillations increases with gamma dosage (Figure 3). For all irradiation doses, the oscillations in these cells typically showed many peaks and were undamped. The mean amplitude and period of oscillations in individual cells did not appear to significantly depend on irradiation level (Supplementary Figure S5).

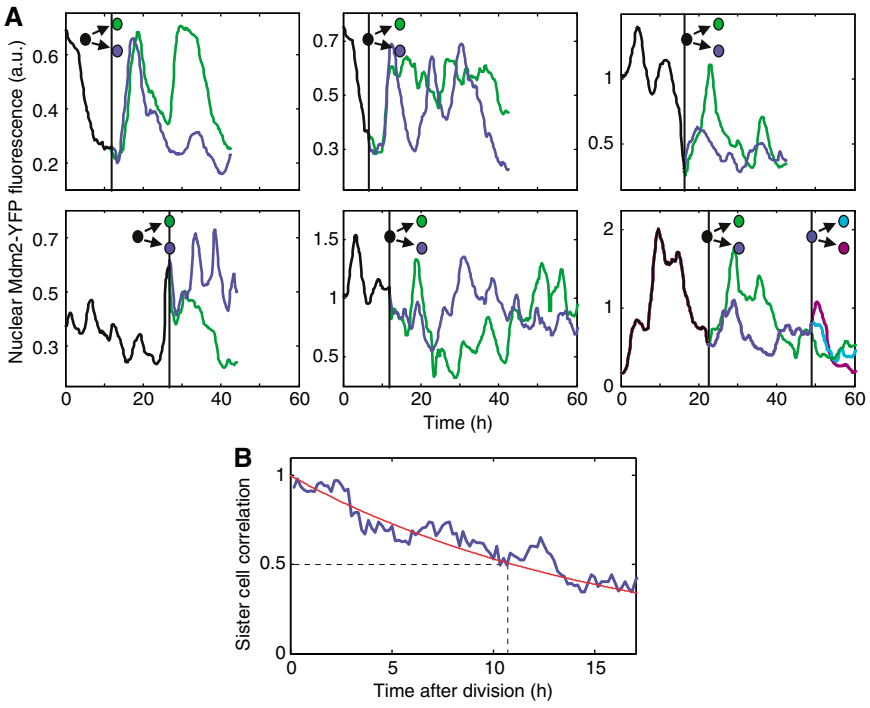

Figure 5 Dynamics of nuclear Mdm2-YFP fluorescence in sister cells. (**A**) Mdm2-YFP fluorescence intensity dynamics in cells that undergo division during the movie. Mdm2-YFP fluorescence is shown in black before division, and in blue and green in the two daughter cells. One of the cells in the bottom right panel undergoes a second division, and the second-generation cells are shown in cyan and purple. The top three panels show cells exposed to 0.3 Gy of gamma irradiation (at time zero), and the bottom three panels show cells exposed to 5 Gy of gamma irradiation. (**B**) Average correlation between 112 sister-cell pairs (normalized mean difference in rank, see Materials and methods) as a function of time following division. Red line: exponential fit, $C=2^{-t/\tau}$, with $\tau=11$ h.

Several families of models can generate the observed oscillations and show consensus biochemical parameter values

We considered several mathematical models of the p53–Mdm2 feedback loop. Since current knowledge of the system is incomplete, we analyzed the simplest possible models, aiming to understand the general properties of model families. Our motivation was to find a simple model that could capture the characteristics of the undamped and noisy oscillations that were found in many of the cells.

We examined six model families (Figure 6A and Table I). All of the models include the negative feedback loop in which p53, denoted by x, transcriptionally activates Mdm2 denoted by y. Active Mdm2 increases the degradation rate of p53.

Three of the models are delay oscillators (I, III and IV) (Mihalas *et al*, 2000; Goldbeter, 2002; Tiana *et al*, 2002; Monk, 2003). The models differ in mathematical details that describe the delay between x and y and the effects of y on x. Model I includes an Mdm2 precursor, denoted by y_0, representing, for example, Mdm2 mRNA, and the action of y on x is described by first-order kinetics in both x and y. In model IV, the action of y on x is nonlinear, and described by a saturating Michaelis–Menten function. In model III, the Mdm2 precursor y_0 is replaced by a stiff delay term, which makes the production rate of Mdm2 depend directly on the concentration of p53 at an earlier time. A recent model by Ma *et al* (2005) and Wagner *et al* (2005) combines features of models III and IV.

In addition to the three delay oscillators, we also considered two relaxation oscillators (II and V) (Wilhelm and Heinrich, 1995; Murray, 2003; Pomerening *et al*, 2003; Tyson *et al*, 2003; Ciliberto *et al*, 2005). In these models, the negative feedback loop is supplemented by a positive feedback loop on p53. This positive feedback loop might represent in a simplified manner the action of additional p53 system components, which have a total upregulating effect on p53 (Harris and Levine, 2005). This type of model was recently studied by Ciliberto *et al* (2005). We considered both linear positive regulation (model V) and nonlinear regulation based on a saturating function (model II).

These models (I–V), although differing in detail, rely on a single negative feedback loop. The last model (VI) is a novel checkpoint mechanism, which uses two negative feedback loops, one direct feedback and one longer loop that impinges on an upstream regulator of p53. In this model, a protein downstream of p53 inhibits a signaling protein that is upstream of p53 (see more details in Supplementary information; Banin *et al*, 1998). For simplicity, this inhibitor is modeled by y, but it need not be Mdm2 and can also represent a different protein with similar dynamics. This model predicts that upstream elements (e.g. phosphorylated ATM) also undergo oscillatory dynamics (see appendix in Supplementary information and Supplementary Figure S9). The model was inspired by the observation that an upstream regulator of p53, namely phosphorylated ATM (Bakkenist and Kastan, 2003) that responds to double-stranded DNA breaks (DSBs), shows a pulse of activity after application of a radiomimetic drug (NCS) in a set of Western blot experiments measuring protein dynamics for 6 h after damage (Banin *et al*, 1998; Stommel and Wahl, 2004).

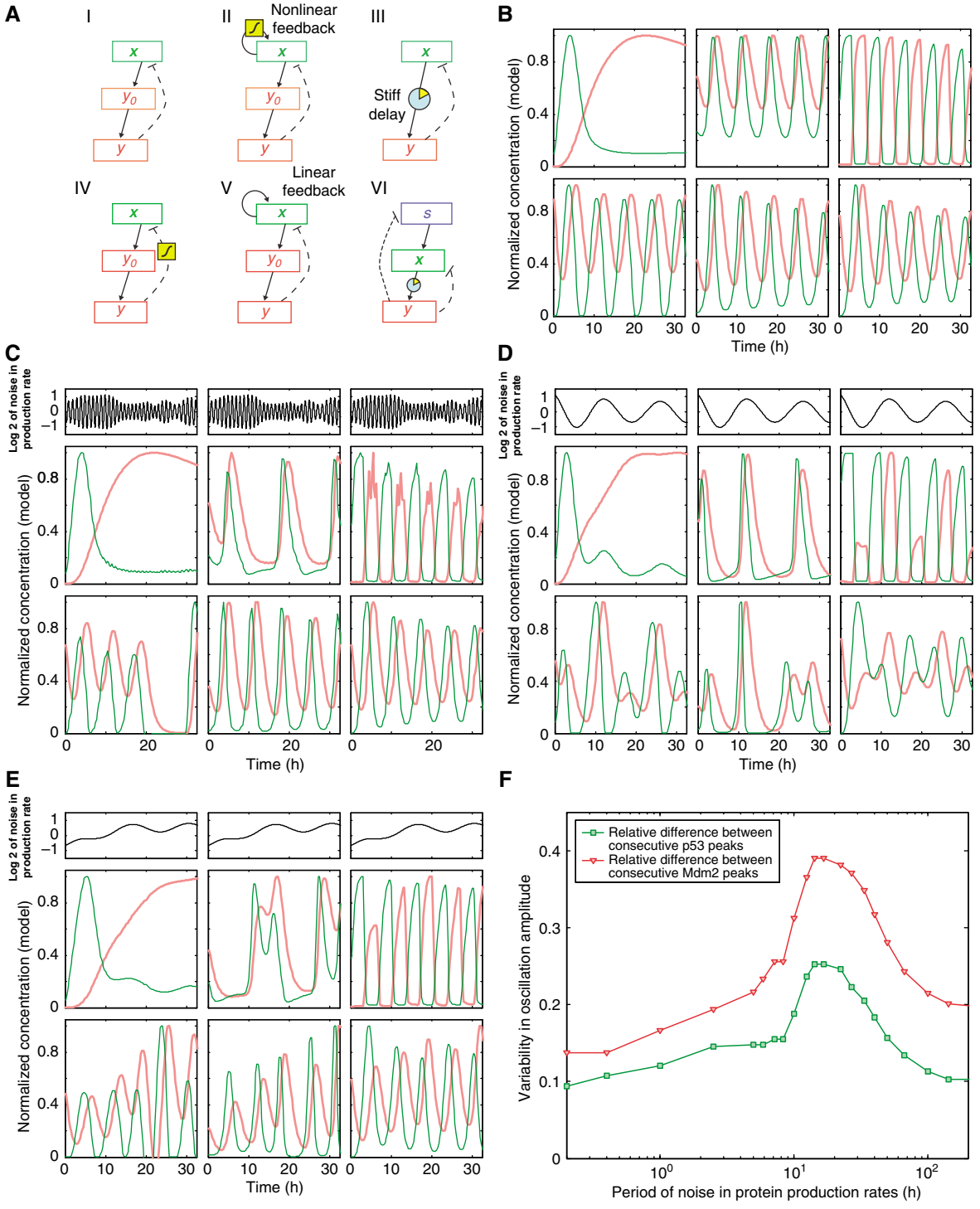

Figure 6 Models of the p53–Mdm2 feedback loop. (**A**) The six families of models (see text and Table I). (**B**) The deterministic or 'noise-free' dynamics obtained by the models, using parameters and initial conditions in Table II, with $\xi(t)=1$. Panels are ordered as in part A. (**C–E**) Examples of the dynamics obtained by these models with noise in protein production rates, $\xi(t)$. The noise $\xi(t)$, which was used for each run, was identical for all models, and is shown for each run in the top panels. The noise was generated as a Gaussian wave-packet with random phases (Supplementary Figure S7), with periods centered around 1 h (C), 12.5 h (D), and 50 h (E), with mean $(\log[\xi(t)])=0$, $\mathrm{STD}(\log[\xi(t)])=0.4$, and $\mathrm{STD}(\xi(t))\approx 0.5$. (**F**) Averaged relative difference between amplitudes of consecutive peaks ($\Delta h/\langle h\rangle$) in simulations of model VI, as a function of noise period.

We numerically solved all six models for a wide range of parameters. We selected parameter values (Table II) that best reproduce an effective averaged individual cell measurements of nuclear p53-CFP and Mdm2-YFP following gamma irradiation, that is, oscillations that do not dampen out considerably and have constant inter-peak timing (Supplementary Figure S6). Note that this effective individual cell dynamics is different from the population-average

Table I

Definitions

Dynamic variables represent levels (concentrations) of
x—nuclear p53
y_0—Mdm2 precursor
y—nuclear Mdm2
S—active signal

ξ—time-dependent noise in protein production rates, $\langle \xi \rangle = 1$

Common parameters

β_x—p53 production rate
β_y—p53-dependent Mdm2 production rate
α_x—Mdm2-independent p53 degradation rate
α_y—Mdm2 degradation rate
α_0—Mdm2 maturation rate
τ—delay in Mdm2 accumulation
α_{xy}—Mdm2-dependent p53 degradation rate

Additional parameters

M, x_{max}, x_{min}—parameters for the piecewise-linear p53 autoregulation
k—p53 threshold for deg. by Mdm2
α_k—saturating p53 degradation rate
Γ—linear p53 production rate
α_S—Mdm2-dependent signal inactivation rate
β_S—constant activation rate of signal (when damage is present)
n—cooperativity of signal

Model equations

Model I

$$\dot{x} = \beta_x \xi - \alpha_x x - \alpha_{xy} y x$$
$$\dot{y}_0 = \beta_y x \xi - \alpha_0 y_0$$
$$\dot{y} = \alpha_0 y_0 - \alpha_y y$$

($\dot{x}$ is the time derivative of x)

Model II

$$\dot{x} = f(x)\xi - \alpha_x x - \alpha_{xy} y x$$
$$\dot{y}_0 = \beta_y x \xi - \alpha_0 y_0$$
$$\dot{y} = \alpha_0 y_0 - \alpha_y y$$

$$f(x) = \begin{cases} \beta_x & \text{for} \quad x \geqslant x_{max} \\ \frac{\beta_x}{M} & \text{for} \quad x \leqslant x_{min} \\ \frac{\beta_x}{M}\left[1 + (M-1)\frac{x - x_{min}}{x_{max} - x_{min}}\right] & \text{for} \quad x_{min} < x < x_{max} \end{cases}$$

Model III

$$\dot{x} = \beta_x \xi - \alpha_x x - \alpha_{xy} y x$$
$$\dot{y} = \beta_y x(t-\tau)\xi - \alpha_y y$$

Model IV

$$\dot{x} = \beta_x \xi - \alpha_x x - \alpha_k y \frac{x}{x+k}$$
$$\dot{y}_0 = \beta_y x \xi - \alpha_0 y_0$$
$$\dot{y} = \alpha_0 y_0 - \alpha_y y$$

Model V

$$\dot{x} = \Gamma x \xi - \alpha_{xy} y x$$
$$\dot{y}_0 = \beta_y x \xi - \alpha_0 y_0$$
$$\dot{y} = \alpha_0 y_0 - \alpha_y y$$

Model VI

$$\dot{x} = \beta_x \frac{S^n}{S^n + 1} \xi - \alpha_{xy} y x$$
$$\dot{y} = \beta_y x(t-\tau)\xi - \alpha_y y$$
$$\dot{S} = \beta_S - \alpha_S y S$$

dynamics, which is a damped oscillation (Supplementary Figure S2E).

Model I cannot produce multiple oscillations similar to those experimentally observed. The oscillations in models II and III are very sensitive to parameters. Small changes in some of the parameters listed in Table II cause these models to show strongly damped oscillations (Supplementary Figure S8). Such sensitive (non-robust) circuits might not be expected to function properly in the noisy cellular context (Savageau, 1976; Barkai and Leibler, 1997; Alon *et al*, 1999; Eldar *et al*, 2002; Kitano, 2004).

In contrast, models IV–VI could generate sustained or weakly damped oscillations (Figure 6B and Supplementary Figure S6) over a broad range of parameters (Supplementary Figure S8). Importantly, most of the parameters shared by all three models showed very similar best-fit values. Thus, these models may provide estimates of the effective biochemical parameters such as production rates and degradation times of p53 and Mdm2. The 'consensus' values of the parameters are shown in Table II. In all three models, the Mdm2 degradation rate was about $\alpha_y \approx 1\,h^{-1}$, the time for Mdm2 maturation was about $1/\alpha_0 \approx \tau \approx 1$ h, and the Mdm2-independant degradation rate of p53, α_x, was negligible. The models also agreed on the values β_x and β_y, the rates of p53 and Mdm2 production.

Increasing the Mdm2 lifetime or its maturation time led, according to the models, to a lower natural frequency and to pulses with longer time periods (Supplementary Figure S8). This might help explain the low-frequency fluctuations observed with no gamma irradiation (Figure 2C), because Mdm2 lifetime is longer in the absence of DNA damage than in its presence (Stommel and Wahl, 2004).

The observed noise in oscillation amplitude is captured by low-frequency fluctuations in the protein production rates

Deterministic simulations cannot capture the variability in the oscillation amplitudes observed in the cells (Figures 1, 2, and 4). We therefore added internal stochasticity to the equations. We found that the characteristic variability observed in our experiments, where amplitude varies more strongly than frequency, could best be captured by varying the protein production rates. Production rate variations change amplitudes, but do not significantly affect the oscillation period (Supplementary Figure S8). In contrast, we find that variations in other parameters, such as degradation rates, generally lead to variations in both amplitude and period.

To describe stochasticity in protein production rates, we used multiplicative noise in the protein production terms.

Table II Model parameters

Common params. & definitions		Units	I	II	III	IV	V	VI	Consensus
β_x	p53 production rate	$P_{max}h^{-1}$	0.3	2.55	2.3	0.9±35%	–	0.9±60%	0.9
β_y	p53-dependent Mdm2 production rate	$M_{max}h^{-1}$ $P_{max}h^{-1}$	0.4	0.85	24	1.1±55%	1.5±60%	1.0±10%	1.2
α_x	Mdm2-independent p53 degradation rate	h^{-1}	0	0.1	0	0 (<<1)	–	–	0
α_y	Mdm2 degradation rate	h^{-1}	0.1	0.6	24	0.8±25%	0.9±30%	0.7±20%	0.8
α_0	Mdm2 maturation rate	h^{-1}	0.1	55	–	0.8±20%	1.1±25%	–	0.9
τ	Delay in Mdm2 accumulation	h	–	–	3.3	–	–	0.9±25%	0.9
α_{xy}	Mdm2-dependent p53 degradation rate	$M_{max}^{-1}h^{-1}$	3.2	3.15	120	–	3.7±50%	1.4±20%	
Additional parameters (see definitions, Table I)				x_{max}= 0.92 P_{max} x_{min} = 0.12 P_{max} M = 34		k= 0.0001 P_{max} (<<1) α_k = 1.7± 20% P_{max} $M_{max}^{-1}h^{-1}$	Γ=2.0 ±25% h^{-1}	α_S=2.7±30% $M_{max}^{-1}h^{-1}$ β_S = 0.9 ±25% K_S n=4	
Initial conditions:	x		0	0.28	0.02	0	0.02	0	
	y_0		0	0	–	0.1	0.2	–	
	y		0	0.73	0.02	0.8	0.5	0.9	
	S							0	

'Best-fit' model parameters used to generate simulations in Figure 6. Models IV–VI, which could be robustly fit to the average dynamics, are highlighted in gray. Parameters with 'consensus' values are highlighted in yellow. Time is in units of hours. p53 and Mdm2 are in units of their maximal nuclear concentrations P_{max} and M_{max}: Signal levels 'S' are in units of its response threshold K_S. Errors are in %.

Most previous theoretical analyses of noise employed white noise, which is rapidly fluctuating (McAdams and Arkin, 1997; Thattai and van Oudenaarden, 2001; Paulsson, 2004; Kaern *et al*, 2005; Ramanathan and Swain, 2005). We used, in addition to white noise, noise with different characteristic correlation times, including noise that varies on slow timescales. This was inspired by the recent observation that protein production rates vary significantly between individual bacterial cells, and that this variation has long autocorrelation times on the order of a cell generation (Rosenfeld *et al*, 2005).

We first used high-frequency noise (similar to white noise), in which the production rates varied with a correlation time on the order of minutes to an hour (Figure 6C). This may represent intrinsic noise due to stochastic transcription and translation (McAdams and Arkin, 1997; Thattai and van Oudenaarden, 2001; Elowitz *et al*, 2002; Ozbudak *et al*, 2002; Blake *et al*, 2003; Isaacs *et al*, 2003; Paulsson, 2004; Becskei *et al*, 2005; Colman-Lerner *et al*, 2005; Golding *et al*, 2005; Kaern *et al*, 2005; Volfson *et al*, 2006). The stronger the noise in production rates, the higher the resulting fluctuations in the dynamics. However, even very strong high-frequency noise (STD of 50% in production rates) resulted in only mild variations in the oscillation amplitudes in all six models. These variations were significantly lower than the variations observed in individual cell measurements in the present experiments.

We next introduced low-frequency noise, with a timescale of several hours (e.g. 12.5 h; Figure 6D). We found that under such noise, the amplitudes vary far more strongly than under high-frequency noise. The extent of the variability was similar to that experimentally observed, with strong amplitude variations and smaller variations in the period of the oscillations.

Finally, we found that very low-frequency noise (e.g. 50 h; Figure 6E) does not produce strong variability in the oscillations. It appears that the oscillators can only amplify the frequency component of the noise close to their natural resonant frequency (about 6 h). We find that the variability is maximal at noise frequencies of about twice the natural frequency of the oscillator (Figure 6F), such that consecutive peaks are oppositely affected by the noise.

The models with low-frequency noise in the production rates showed qualitatively similar dynamics to those found in the experiments, including occasional loss of a peak. Only model VI was able to reproduce our observations that p53 and Mdm2 peak amplitudes had only a weak correlation. Other models had a strong coupling in the variations of the peaks of these two proteins.

Discussion

The present study examined p53 and Mdm2 dynamics in individual cells from a clone. We found undamped oscillations with more than 10 consecutive peaks, lasting for at least three days following DNA damage. The dynamics showed striking cell–cell variability. A fraction of the cells showed either no response or a slowly fluctuating signal. The cells that performed oscillations displayed large variation in peak amplitude, and smaller variations in the oscillation period. Models point to the source of the noise in the oscillations: low-frequency fluctuations in protein production rates.

The oscillations following DNA-damaging gamma irradiation had a period of about 5.5 h, and were synchronized to the gamma irradiation pulse. The number of oscillating cells increased with gamma dose, reaching about 60% of the cells following 10 Gy. Some cells divided during the movies. Divisions allowed one to follow the passage of information across the cell division event. We found that the oscillations continued in the same phase after division, suggesting that the information in the system is transferred to the daughter cells. However, correlation between daughter cells was lost after about 11 h. This loss of correlation indicates the timescale on which prediction of the cell state in this system can be made based on the cell state in the past.

The oscillations after DNA damage had a distinct noise characteristic. Their amplitudes varied from peak to peak by about 70%. In contrast to the large amplitude variation, the oscillation period was less noisy, and had a variability of only 20%. Similar features are seen in other biological oscillators. For example, the cell-autonomous circadian clock in cyanobacteria and in fibroblasts shows larger amplitude variations than timing variations in experiments and in models (Barkai and Leibler, 2000; Vilar *et al*, 2002; Mihalcescu *et al*, 2004; Nagoshi *et al*, 2004). Precise period and variable amplitude may characterize other biological oscillators.

Although the timing is relatively precise, and the oscillations are initially synchronized to the gamma irradiation signal, the variation in timing causes peaks to eventually go out of phase. Therefore, the p53 and Mdm2 dynamics appear as damped oscillations in assays that average over cell populations, such as immunoblots. This averaging effect was also seen by averaging over the present individual cell dynamics, showing damped oscillations with 2–3 discernable peaks (Supplementary Figure S2E).

It is interesting to compare the present results with our previous study that followed cells over only 16 h (Lahav *et al*, 2004). In that study, cells showed either zero, one, or two peaks of p53 in the 16 h period. The fraction of cells with two peaks increased with gamma irradiation. It seemed therefore that the *number* of peaks depended on the gamma dose. The present study, which followed cells over a much longer time, suggests that oscillations in most cells are in fact long lasting, and that most oscillating cells show numerous peaks following damage. We found that the *fraction* of oscillating cells (with a 4–7 h period in Mdm2-YFP levels) increases with gamma dose. The previous 16 h movies registered some cells with one pulse, whereas the present study indicates that such cells can often show additional pulses after a delay (Supplementary Figure S4). This emphasizes the importance of extended measurements for dynamical systems with slow timescales.

How are the oscillations produced? Instead of analyzing a single model, the limited state of current knowledge of the system makes it appropriate to study several families of models, to ask about the general properties of the dynamics. We performed a theoretical analysis of several model families. Most models were able to produce oscillations. The models suggest that the noise in the oscillations is owing to stochasticity in the protein production rates, rather than in other parameters such as degradation rates. Furthermore, the observed oscillations suggest that the noise in protein production rate has a slowly varying component, with a correlation time of 10–20 h. Internal noise that is too fast or too slow cannot explain the observed variability. The negative feedback loop, which is a natural oscillator, amplifies the frequency component of the noise in the vicinity of its natural frequency, resulting in the observed variability.

The present results were obtained in a clonal population of a human, MCF7 cell line, stably expressing fluorescent fusions of p53 and Mdm2. Endogenous p53 and Mdm2 oscillations were found in cell averages also in MCF7 cells that do not express ectopic fusion proteins (Lev Bar-Or *et al*, 2000). These cancer cells might be deficient in some aspects of p53 regulation (Vojtesek and Lane, 1993) and downstream apoptotic responses (Janicke *et al*, 1998). It would therefore be important to study other cell types. For example, Western blots performed over several hours after DNA damage showed a peak of p53, Mdm2, and p21 expression in several cell lines including WS1 human primary skin fibroblasts (Stommel and Wahl, 2004), human glioblastoma cells (Ohnishi *et al*, 1999), and HCT116 human colon cancer cells (Chen *et al*, 2005). This raises the possibility that oscillations may occur also in these cell lines. It would be important to extend the present individual cell experiments to other cell types, and to try to monitor DNA damage in parallel to the dynamics of the p53 system.

Perhaps the most intriguing question raised by these observations is the biological function of the undamped oscillations, assuming that they also occur in normal cells with endogenous p53 and Mdm2. One clue is that undamped oscillations are also found in other stress-response systems. Tightly regulated oscillations with variable amplitude and precise timing were recently observed in the SOS DNA-damage response in *Escherichia coli* (Friedman *et al*, 2005). Highly variable nuclear-cytoplasmic oscillations were found in NF-κB system (Hoffmann *et al*, 2002; Nelson *et al*, 2004). Both NF-κB and the SOS regulator LexA are involved in a negative feedback loop motif similar to that of p53–Mdm2. As in the p53 system, these loops are embedded in many additional interactions. The presence of oscillations in the systems mentioned above may suggest that oscillations play a general role in stress or damage response.

The present study demonstrated prolonged undamped oscillations in the p53–Mdm2 system following gamma irradiation. Significant cell–cell variability was observed in the amplitude but not period of the oscillations. Some of the cells had slow fluctuations that do not resemble oscillations; the fraction of oscillating cells increased with irradiation dose but the oscillation amplitude did not. Modeling suggests that

the noise in the oscillations reflects slow internal noise in protein production rates. The present approach that combines long-term dynamic experiments in individual cells and theoretical analysis of families of models may help to understand oscillations and cell–cell variability in other regulatory systems.

Materials and methods

Cell line and constructs

We used MCF7, human breast cancer epithelial cells, U280, stably transfected with pU265 and pU293 as described (Lahav *et al*, 2004). In pU265, ECFP from pECFP-C1 (Clontech) was subcloned after the last codon of p53 cDNA, under the mouse Metallothionein-1 promoter (MTΔ156) (Brinster *et al*, 1982). This promoter provides a basal and constant level of transcription of p53-CFP. A basal promoter for p53-CFP was chosen because p53 is thought to be primarily regulated at the protein level and not at the transcriptional level (Michael and Oren, 2003). Control experiments with CFP expressed from this promoter showed constant expression with no oscillations. In pU293, the hMDM2 promoter was cloned by PCR using genomic DNA as a template, creating a 3.5 kb fragment upstream of the ATG site in exon 3, including P1 and P2 (Oliner *et al*, 1992). This promoter was subcloned into pEYFP-1 (Clontech) (Lahav, 2004).

Time-lapse microscopy

Cells were maintained at 37°C in 96-well plates or in 2 mm optical plates (Nunc) in RPMI 1640 medium containing 10% fetal calf serum (Sigma). At 1–2 h before observation in the microscope, medium was changed to RPMI 1640 medium containing 3% fetal calf serum, HEPES, and 2 mM L-glutamine, lacking riboflavin and phenol red (Beit Haemek, Biological Industries), in order to reduce background fluorescence. Cells were then exposed to the appropriate dose of gamma irradiation (^{60}Co, 1.8 Gy min^{-1}). The number of DSBs has been found to be linear in gamma dose, with an average of about 30 DSB per Gy per cell (Bonner, 2003). Cells were viewed with three types of inverted fluorescence microscope systems denoted by MS.I, MS.II, and MS.III. MS.I: Olympus IX70 with a Photometrics Quantix 57 cooled back-illuminated CCD camera, in a 37°C incubator, using bright-field, CFP and YFP exposures, every 20 min, with a mercury lamp. MS.II: Leica DMIRE2 with a Hamamatsu ORCA-ER cooled back-illuminated CCD camera, in a 37°C incubator with humidity and CO_2 control, using phase-contrast and YFP exposures only, every 10 min, with a mercury lamp. MS.III: Nikon TE2000E2 with a Hamamatsu ORCA-ER cooled back-illuminated CCD camera, in a 37°C incubator with humidity and CO_2 control, using phase-contrast, YFP and CFP exposures, every 20 min, with a xenon lamp.

CFP filter set: excitation 436/20 nm, dichroic beam splitter 455 nm, emission 480/40 nm. YFP filter set: excitation 500/20 nm, a dichroic beam splitter 515 nm, emission 535/30 nm.

The mean cell generation time was about 20 h in the CO_2 incubated microscope without gamma irradiation. We find that movies using CFP and YFP illumination over 3 days did not visibly affect the cell morphology or generation time.

Cell tracking and fluorescence quantification

Cell images captured in MS.I (Figure 1 and Supplementary Figure S4): Relative fluorescence analysis and background subtraction was carried out using custom written Matlab software (Mathworks Inc.). The location of each cell nucleus was marked manually in each frame, using a custom written graphical user interface in Matlab. Independent tracking by four different researchers showed that this manual step contributed <5% errors. Background fluorescence was measured at manually marked locations with no cells, and subtracted from the nuclear fluorescence. Mean fluorescence intensity of pixels in the nucleus was measured. Cellular autofluorescence of wild-type MCF7 cells without the CFP or YFP genes gave consistent and low values with a mean of 25 CFP fluorescence units per pixel and 1 YFP fluorescence unit per pixel, with a coefficient of variation of ∼30%. In these units, average peak amplitude (range from minimum to maximum) was ∼45 CFP fluorescence units (for p53-CFP) and ∼8 YFP fluorescence units (for Mdm2-YFP).

Cell images captured with MS.II (Figures 2 and 5, and Supplementary Figure S2) and MS.III: Relative fluorescence analysis and background subtraction was carried out using custom written Matlab software (Mathworks Inc.). Nuclei identification and tracking was performed using MetaMorph™ software, and was manually controlled for accuracy. Comparison of sister cells (that were separately tracked) on frames before cell division shows that the identification and tracking contributes ∼2% errors. Background was automatically subtracted. Mean fluorescence intensity of pixels in the nucleus was measured. Autofluorescence (in the YFP channel) was negligible. The inhomogeneity of the illumination was measured using a solution of purified GFP (BD Biosciences Clontech, Palo Alto, CA) before and after every movie and automatically corrected using custom written Matlab software (Mathworks Inc.). Bleaching effects were corrected using an empirical fit of the mean nuclear fluorescence levels to a decaying exponent with an offset. Independent controls, in which H1299 cells with constitutive nuclear YFP expression were imaged, indicate that measurement errors and fluctuations in this system are on the order of a few percent.

Statistical analysis of pulse properties

The p53-CFP and Mdm2-YFP data from MS.I were analyzed in the time domain. In the dynamic curve of each cell, separate pulses of expression were manually marked using custom written software (Matlab). The separate pulses were identified using criteria based on pulse magnitude and signal-to-noise ratio. The baseline was subtracted for each pulse separately, to correct for slowly varying noise in the fluorescence quantification, which may originate from slowly varying autofluorescence of cells. For the comparison of the pulse properties, the time domain was divided into segments of length 300–400 min, and each pulse was independently assigned an ordinal number according to the time segment when it occurs. Average properties (and standard errors) were then calculated for all the pulses that occur at a given time interval (Figure 4 and Supplementary Figure S5).

Pitch detection

The intensity signals from each cell, as obtained from the microscope, were analyzed to detect the oscillation period (1/frequency). We used a standard method for the detection of pitch, used in speech and music processing (Rabiner and Schafer, 1978). Pitch can be considered as the basic frequency of oscillations. Each signal was divided into segments of 128 samples, with a sliding window, which was moved at increments of eight samples. For each window, the autocorrelation of the windowed segment was computed, and normalized so that the autocorrelations at zero lag are identically 1. The first peak of the autocorrelation function was detected and identified as the pitch period of this window if its autocorrelation value was higher than 0.2. The sliding window method enables tracing temporal changes in the oscillation period. To detect the most prominent pitch period for each cell, we binned separate segment periods into 10 bins and selected the most common period.

Sister-cell similarity

At each time point, we ranked all the cells in a movie from lowest to highest nuclear Mdm2-YFP fluorescence level, and normalized the ranking to the range 0–1. For a random pair of cells, the absolute difference in ranking is equal to D_r=1/3 on average. For each pair of sister cells (after division), we measured the absolute difference in rank between the two sister cells. We calculated the average for all sister pairs as a function of time after division, for a total of 112 sister-cell pairs after 0.3, 5, and 10 Gy of gamma irradiation. This average difference, $D(t)$ was found to increase over time from $D(t=0)\sim0.05$

(equivalent to the minimal rank difference in a movie with 20 cells) to $D(t>30\,\mathrm{h})\sim 0.3$, close to the population average between unrelated cells. In Figure 5, we plot the normalized sister-pair difference, $D'(t)=(D_r-D(t))/(D_r-D(0))$. Similar results (half correlation time of 6–16 h) were found with different measures of average sister-cell rank differences, such as root-mean-square difference, and with different subsets of cell (such as only those exposed to 0.3 or 5 Gy).

Model simulation

Numerical integration and optimization were carried out using Matlab software.

Supplementary information

Supplementary information is available at the *Molecular Systems Biology* website (www.nature.com/msb).

Acknowledgements

We thank Michael B Elowitz for assistance and contributions, Arnold J Levine and Moshe Oren for encouragement discussions and suggestions, Gareth L Bond, Gustavo A Stolovitzky, Lan Ma, John M Wagner and all members of our labs for comments and discussions. We acknowledge support grants from the European Commission (COMBIO: LSHGCT-2004-503568) and from the Kahn Fund for Systems Biology at the Weizmann Institute of Science.

References

Alon U (2003) Biological networks: the tinkerer as an engineer. *Science* **301:** 1866–1867

Alon U (2006) *An Introduction to Systems Biology: Design Principles of Biological Circuits*. London, UK: CRC Press

Alon U, Surette MG, Barkai N, Leibler S (1999) Robustness in bacterial chemotaxis. *Nature* **397:** 168–171

Bakkenist CJ, Kastan MB (2003) DNA damage activates ATM through intermolecular autophosphorylation and dimer dissociation. *Nature* **421:** 499–506

Banin S, Moyal L, Shieh S, Taya Y, Anderson CW, Chessa L, Smorodinsky NI, Prives C, Reiss Y, Shiloh Y, Ziv Y (1998) Enhanced phosphorylation of p53 by ATM in response to DNA damage. *Science* **281:** 1674–1677

Barak Y, Juven T, Haffner R, Oren M (1993) mdm2 expression is induced by wild type p53 activity. *EMBO J* **12:** 461–468

Barkai N, Leibler S (1997) Robustness in simple biochemical networks. *Nature* **387:** 913–917

Barkai N, Leibler S (2000) Circadian clocks limited by noise. *Nature* **403:** 267–268

Becskei A, Kaufmann BB, van Oudenaarden A (2005) Contributions of low molecule number and chromosomal positioning to stochastic gene expression. *Nat Genet* **37:** 937–944

Becskei A, Serrano L (2000) Engineering stability in gene networks by autoregulation. *Nature* **405:** 590–593

Blake WJ, Collins JJ (2005) And the noise played on: stochastic gene expression and HIV-1 infection. *Cell* **122:** 147–149

Blake WJ, Kaern M, Cantor CR, Collins JJ (2003) Noise in eukaryotic gene expression. *Nature* **422:** 633–637

Bond GL, Hu W, Levine AJ (2005) MDM2 is a central node in the p53 pathway: 12 years and counting. *Curr Cancer Drug Targets* **5:** 3–8

Bonner WM (2003) Low-dose rediation: thresholds, bystander effects, and adaptive responses. *Proc Natl Acad Sci USA* **100:** 4973–4975

Boyer LA, Lee TI, Cole MF, Johnstone SE, Levine SS, Zucker JP, Guenther MG, Kumar RM, Murray HL, Jenner RG, Gifford DK, Melton DA, Jaenisch R, Young RA (2005) Core transcriptional regulatory circuitry in human embryonic stem cells. *Cell* **122:** 947–956

Brinster RL, Chen HY, Warren R, Sarthy A, Palmiter RD (1982) Regulation of metallothionein–thymidine kinase fusion plasmids injected into mouse eggs. *Nature* **296:** 39–42

Chen L, Gilkes DM, Pan Y, Lane WS, Chen J (2005) ATM and Chk2-dependent phosphorylation of MDMX contribute to p53 activation after DNA damage. *EMBO J* **24:** 3411–3422

Ciliberto A, Novak B, Tyson J (2005) Steady states and oscillations in the p53/Mdm2 network. *Cell Cycle* **4:** 488–493

Colman-Lerner A, Gordon A, Serra E, Chin T, Resnekov O, Endy D, Pesce CG, Brent R (2005) Regulated cell-to-cell variation in a cell-fate decision system. *Nature* **437:** 699–706

Eldar A, Dorfman R, Weiss D, Ashe H, Shilo BZ, Barkai N (2002) Robustness of the BMP morphogen gradient in *Drosophila* embryonic patterning. *Nature* **419:** 304–308

Elowitz MB, Levine AJ, Siggia ED, Swain PS (2002) Stochastic gene expression in a single cell. *Science* **297:** 1183–1186

Friedman N, Vardi S, Ronen M, Alon U, Stavans J (2005) Precise temporal modulation in the response of the SOS DNA repair network in individual bacteria. *PLoS Biol* **3:** e238

Goldbeter A (2002) Computational approaches to cellular rhythms. *Nature* **420:** 238–245

Golding I, Paulsson J, Zawilski SM, Cox EC (2005) Real-time kinetics of gene activity in individual bacteria. *Cell* **123:** 1025–1036

Harris SL, Levine AJ (2005) The p53 pathway: positive and negative feedback loops. *Oncogene* **24:** 2899–2908

Hartwell LH, Hopfield JJ, Leibler S, Murray AW (1999) From molecular to modular cell biology. *Nature* **402:** C47–C52

Hasty J, Dolnik M, Rottschafer V, Collins JJ (2002) Synthetic gene network for entraining and amplifying cellular oscillations. *Phys Rev Lett* **88:** 148101

Haupt Y, Maya R, Kazaz A, Oren M (1997) Mdm2 promotes the rapid degradation of p53. *Nature* **387:** 296–299

Hoffmann A, Levchenko A, Scott ML, Baltimore D (2002) The IκB–NF-κB signaling module: temporal control and selective gene activation. *Science* **298:** 1241–1245

Isaacs FJ, Hasty J, Cantor CR, Collins JJ (2003) Prediction and measurement of an autoregulatory genetic module. *Proc Natl Acad Sci USA* **100:** 7714–7719

Janicke RU, Sprengart ML, Wati MR, Porter AG (1998) Caspase-3 is required for DNA fragmentation and morphological changes associated with apoptosis. *J Biol Chem* **273:** 9357–9360

Kaern M, Elston TC, Blake WJ, Collins JJ (2005) Stochasticity in gene expression: from theories to phenotypes. *Nat Rev Genet* **6:** 451–464

Kalir S, Alon U (2004) Using a quantitative blueprint to reprogram the dynamics of the flagella gene network. *Cell* **117:** 713–720

Kitano H (2004) Biological robustness. *Nat Rev Genet* **5:** 826–837

Kubbutat MH, Jones SN, Vousden KH (1997) Regulation of p53 stability by Mdm2. *Nature* **387:** 299–303

Kubbutat MH, Vousden KH (1998) Keeping an old friend under control: regulation of p53 stability. *Mol Med Today* **4:** 250–256

Lahav G (2004) The strength of indecisiveness: oscillatory behavior for better cell fate determination. *Sci STKE* **2004:** pe55

Lahav G, Rosenfeld N, Sigal A, Geva-Zatorsky N, Levine AJ, Elowitz MB, Alon U (2004) Dynamics of the p53–Mdm2 feedback loop in individual cells. *Nat Genet* **36:** 147–150

Larkin ND, Jackson SP (1999) Regulation of p53 in response to DNA damage. *Oncogene* **18:** 7644–7655

Lee TI, Rinaldi NJ, Robert F, Odom DT, Bar-Joseph Z, Gerber GK, Hannett NM, Harbison CT, Thompson CM, Simon I, Zeitlinger J, Jennings EG, Murray HL, Gordon DB, Ren B, Wyrick JJ, Tagne JB, Volkert TL, Fraenkel E, Gifford DK, Young RA (2002) Transcriptional regulatory networks in *Saccharomyces cerevisiae*. *Science* **298:** 799–804

Lev Bar-Or R, Maya R, Segel LA, Alon U, Levine AJ, Oren M (2000) Generation of oscillation by the p53–Mdm2 feedback loop: a theoretical and experimental study. *Proc Natl Acad Sci USA* **97:** 11250–11255

Ma L, Wagner J, Rice JJ, Hu W, Levine AJ, Stolovitzky GA (2005) A plausible model for the digital response of p53 to DNA damage. *Proc Natl Acad Sci USA* **102:** 14266–14271

Ma'ayan A, Jenkins SL, Neves S, Hasseldine A, Grace E, Dubin-Thaler B, Eungdamrong NJ, Weng G, Ram PT, Rice JJ, Kershenbaum A, Stolovitzky GA, Blitzer RD, Iyengar R (2005) Formation of regulatory patterns during signal propagation in a mammalian cellular network. *Science* **309:** 1078–1083

Mangan S, Alon U (2003) Structure and function of the feed-forward loop network motif. *Proc Natl Acad Sci USA* **100:** 11980–11985

Mangan S, Itzkovitz S, Zaslaver A, Alon U (2006) The incoherent feed-forward loop accelerates the response-time of the gal system of *Escherichia coli*. *J Mol Biol* **356:** 1073–1081

McAdams HH, Arkin A (1997) Stochastic mechanisms in gene expression. *Proc Natl Acad Sci USA* **94:** 814–819

McAdams HH, Arkin A (1999) It's a noisy business! Genetic regulation at the nanomolar scale. *Trends Genet* **15:** 65–69

Meek DW (2004) The p53 response to DNA damage. *DNA Repair (Amst)* **3:** 1049–1056

Michael D, Oren M (2003) The p53–Mdm2 module and the ubiquitin system. *Semin Cancer Biol* **13:** 49–58

Mihalas GI, Simon Z, Balea G, Popa E (2000) Possible oscillatory behavior in p53–Mdm2 interaction computer simulation. *J Biol Syst* **8:** 21–29

Mihalcescu I, Hsing W, Leibler S (2004) Resilient circadian oscillator revealed in individual cyanobacteria. *Nature* **430:** 81–85

Milo R, Shen-Orr S, Itzkovitz S, Kashtan N, Chklovskii D, Alon U (2002) Network motifs: simple building blocks of complex networks. *Science* **298:** 824–827

Momand J, Wu HH, Dasgupta G (2000) MDM2—master regulator of the p53 tumor suppressor protein. *Gene* **242:** 15–29

Monk NA (2003) Oscillatory expression of Hes1, p53, and NF-kappaB driven by transcriptional time delays. *Curr Biol* **13:** 1409–1413

Murray JD (2003) *Mathematical Biology*, 3rd edn. New York: Springer-Verlag

Nagoshi E, Saini C, Bauer C, Laroche T, Naef F, Schibler U (2004) Circadian gene expression in individual fibroblasts: cell-autonomous and self-sustained oscillators pass time to daughter cells. *Cell* **119:** 693–705

Nelson DE, Ihekwaba AEC, Elliott M, Johnson JR, Gibney CA, Foreman BE, Nelson G, See V, Horton CA, Spiller DG, Edwards SW, McDowell HP, Unitt JF, Sullivan E, Grimley R, Benson N, Broomhead D, Kell DB, White MRH (2004) Oscillations in NF-{kappa}B signaling control the dynamics of gene expression. *Science* **306:** 704–708

Novick A, Weiner M (1957) Enzyme induction as an all-or-none phenomenon. *Proc Natl Acad Sci USA* **43:** 553–566

Odom DT, Zizlsperger N, Gordon DB, Bell GW, Rinaldi NJ, Murray HL, Volkert TL, Schreiber J, Rolfe PA, Gifford DK, Fraenkel E, Bell GI, Young RA (2004) Control of pancreas and liver gene expression by HNF transcription factors. *Science* **303:** 1378–1381

Ohnishi T, Wang X, Takahashi A, Ohnishi K, Ejima Y (1999) Low-dose-rate radiation attenuates the response of the tumor suppressor TP53. *Radiat Res* **151:** 368–372

Oliner JD, Kinzler KW, Meltzer PS, George DL, Vogelstein B (1992) Amplification of a gene encoding a p53-associated protein in human sarcomas. *Nature* **358:** 80–83

Oren M (2003) Decision making by p53: life, death and cancer. *Cell Death Differ* **10:** 431–442

Ozbudak EM, Thattai M, Kurtser I, Grossman AD, van Oudenaarden A (2002) Regulation of noise in the expression of a single gene. *Nat Genet* **31:** 69–73

Paulsson J (2004) Summing up the noise in gene networks. *Nature* **427:** 415–418

Piette J, Neel H, Marechal V (1997) Mdm2: keeping p53 under control. *Oncogene* **15:** 1001–1010

Pomerening JR, Sontag ED, Ferrell Jr JE (2003) Building a cell cycle oscillator: hysteresis and bistability in the activation of Cdc2. *Nat Cell Biol* **5:** 346–351

Prives C (1998) Signaling to p53: breaking the MDM2–p53 circuit. *Cell* **95:** 5–8

Prives C, Hall PA (1999) The p53 pathway. *J Pathol* **187:** 112–126

Rabiner LR, Schafer RW (1978) *Digital Processing of Speech Signals*, 1st edn. Englewood Cliffs, NJ: Prentice-Hall

Ramanathan S, Swain PS (2005) Tracing the sources of cellular variation. *Dev Cell* **9:** 576–578

Raser JM, O'Shea EK (2004) Control of stochasticity in eukaryotic gene expression. *Science* **304:** 1811–1814

Raser JM, O'Shea EK (2005) Noise in gene expression: origins, consequences, and control. *Science* **309:** 2010–2013

Rosenfeld N, Young JW, Alon U, Swain PS, Elowitz MB (2005) Gene regulation at the single-cell level. *Science* **307:** 1962–1965

Ryan KM, Phillips AC, Vousden KH (2001) Regulation and function of the p53 tumor suppressor protein. *Curr Opin Cell Biol* **13:** 332–337

Sachs K, Perez O, Pe'er D, Lauffenburger DA, Nolan GP (2005) Causal protein-signaling networks derived from multiparameter single-cell data. *Science* **308:** 523–529

Savageau MA (1976) *Biochemical Systems Analysis: A Study of Function and Design in Molecular Biology*. Cambridge, MA: Addison-Wesley Pub. Co

Shen-Orr SS, Milo R, Mangan S, Alon U (2002) Network motifs in the transcriptional regulation network of *Escherichia coli*. *Nat Genet* **31:** 64–68

Spudich JL, Koshland Jr DE (1976) Non-genetic individuality: chance in the single cell. *Nature* **262:** 467–471

Stommel JM, Wahl GM (2004) Accelerated MDM2 auto-degradation induced by DNA-damage kinases is required for p53 activation. *EMBO J* **23:** 1547–1556

Thattai M, van Oudenaarden A (2001) Intrinsic noise in gene regulatory networks. *Proc Natl Acad Sci USA* **98:** 8614–8619

Tiana G, Jensen MH, Sneppen K (2002) Time delay as a key to apoptosis induction in the p53 network. *Eur Phys J B* **29:** 135–140

Tyson JJ (2004) Monitoring p53's pulse. *Nat Genet* **36:** 113–114

Tyson JJ, Chen KC, Novak B (2003) Sniffers, buzzers, toggles and blinkers: dynamics of regulatory and signaling pathways in the cell. *Curr Opin Cell Biol* **15:** 221–231

Vilar JM, Kueh HY, Barkai N, Leibler S (2002) Mechanisms of noise-resistance in genetic oscillators. *Proc Natl Acad Sci USA* **99:** 5988–5992

Vogelstein B, Lane D, Levine AJ (2000) Surfing the p53 network. *Nature* **408:** 307–310

Vojtesek B, Lane DP (1993) Regulation of p53 protein expression in human breast cancer cell lines. *J Cell Sci* **105** (Part 3)**:** 607–612

Volfson D, Marciniak J, Blake WJ, Ostroff N, Tsimring LS, Hasty J (2006) Origins of extrinsic variability in eukaryotic gene expression. *Nature* **439:** 861–864

Vousden KH, Lu X (2002) Live or let die: the cell's response to p53. *Nat Rev Cancer* **2:** 594–604

Wagner J, Ma L, Rice JJ, Hu W, Levine AJ, Stolovitzky GA (2005) p53–Mdm2 loop controlled by a balance of its feedback strength and effective dampening using ATM and delayed feedback. *IEE Proc Syst Biol* **152:** 109–118

Weinberger LS, Burnett JC, Toettcher JE, Arkin AP, Schaffer DV (2005) Stochastic gene expression in a lentiviral positive-feedback loop: HIV-1 Tat fluctuations drive phenotypic diversity. *Cell* **122:** 169–182

Wilhelm T, Heinrich R (1995) Smallest chemical-reaction system with Hopf-bifurcation. *J Math Chem* **17:** 1–14

Wu X, Bayle JH, Olson D, Levine AJ (1993) The p53–mdm-2 autoregulatory feedback loop. *Genes Dev* **7:** 1126–1132

Yeger-Lotem E, Sattath S, Kashtan N, Itzkovitz S, Milo R, Pinter RY, Alon U, Margalit H (2004) Network motifs in integrated cellular networks of transcription-regulation and protein–protein interaction. *Proc Natl Acad Sci USA* **101:** 5934–5939